mathematics

MDPI

Article

Mitigation of the Collision Risk of a Virtual Impactor Based on the 2011 AG5 Asteroid Using a Kinetic Impactor

Marco Cinelli

Istituto di Astrofisica e Planetologia Spaziali (IAPS)—Istituto Nazionale di Astrofisica (INAF), 00133 Rome, Italy; marco.cinelli@inaf.it

Abstract: In recent years, the escalating risk of natural disasters caused by Near-Earth Objects (NEOs) has garnered heightened scrutiny, particularly in the aftermath of the 2013 Chelyabinsk event. This has prompted increased interest from governmental and supranational entities, leading to the formulation of various measures and strategies aimed at mitigating the potential threat posed by NEOs. This paper delves into the analysis of the 2011 AG5 asteroid within the context of small celestial bodies (e.g., asteroids, comets, or meteoroids) exhibiting resonant orbits with Earth's heliocentric revolution. Initial observations in 2011 raised alarms regarding the asteroid's orbital parameters, indicating a significant risk of Earth impact during its resonant encounter in 2040. Subsequent observations, however, mitigated these concerns. Here, we manipulate the orbital elements of the 2011 AG5 asteroid to simulate its behavior as a virtual impactor (a virtual asteroid whose orbit could impact Earth). This modification facilitates the assessment of impact mitigation resulting from a deflection maneuver utilizing a kinetic impactor. The deflection maneuver, characterized as an impulsive change in the asteroid's momentum, is executed during a resonant encounter occurring approximately two decades before the potential impact date. The paper systematically evaluates the dependence of the deflection maneuver's efficacy on critical parameters, including the position along the orbit, epoch, and momentum enhancement factor.

Keywords: kinetic impactor; potential hazardous asteroids; Near-Earth Objects; asteroid deflection

PACS: 96.30.Ys

MSC: 70F05

Citation: Cinelli, M. Mitigation of the Collision Risk of a Virtual Impactor Based on the 2011 AG5 Asteroid Using a Kinetic Impactor. *Mathematics* **2024**, *12*, 378. https://doi.org/10.3390/math12030378

Academic Editor: Manuel De León

Received: 13 December 2023
Revised: 17 January 2024
Accepted: 21 January 2024
Published: 24 January 2024

1. Introduction

In recent decades, the international community has increasingly considered strategies to control and mitigate the risk of natural disasters caused by the potential impact of Near-Earth Objects (NEOs) on Earth's surface. The Chelyabinsk event occurred on 15 February 2013, when a small asteroid with a diameter of ∼20 m [1] unexpectedly hit the territories at the foot of the Ural Mountains, releasing energy equivalent to that of 500 kton of TNT and causing injuries to approximately 1500 people [2], further highlighting the problem. The Chelyabinsk event is not an exception; going back just over a century, we can recall the impact of the Tunguska bolide that, on 30 June 1908, with its 60 m diameter, caused an explosion estimated to be between 10 and 40 megatons and leveled more than 2000 km^2 of Siberian forest [3]. Lastly, the most famous and certainly the most catastrophic event for life on Earth cannot be ignored, that of Chicxulub in the Yucatán Peninsula, where, 65 million years ago, the impact of an object with a diameter estimated to be greater than 10 km caused the extinction of dinosaurs and more than 70% of the species that then lived on the planet [4].

Statistics indicate that impacts of asteroids with diameters greater than 1 km, which can have catastrophic effects on a global scale, occur about every 500,000 years [5]. Meanwhile,

impacts of objects larger than 100 m, which can cause significant damage on a regional scale, occur about every 10,000 years [6]. Therefore, it is easy to understand the growing interest in the topic in recent years, even at the institutional level. The European Union created the NEOShield project in 2012, through which several tools have been developed to assess impact risks and design strategies to deflect PHAs (potential hazardous asteroids) [7]. The term PHAs refers to asteroids with a perihelion of less than 1.3 AU (astronomical unit), apparent magnitudes $H \leq 22$ (i.e., a diameter exceeding approximately 140 m, assuming a mean Near-Earth Object albedo of 0.14, as determined by [8]), and a minimum orbit intersection distance (MOID) of within 0.05 AU of Earth's orbit [9]. Based on this definition, considering a time horizon of 100 years, it is possible to count a number of PHAs (with a nonzero chance of impact) of at least 10,000 units. The United Nations, through its commission dedicated to regulating access to space, UN COPUOS (United Nations Committee on the Peaceful Uses of Outer Space), has repeatedly addressed the issue: during the 56th UN COPUOS congress, a 2-year program was created to mitigate the threat of PHAs [10]. Finally, the United States Congress assigned NASA to catalog at least 90% of PHAs with diameters equal to or greater than 140 m by 2020 [11].

Risk mitigation strategies consist of two phases. The first stage is dedicated to the identification, cataloging, observation, and analysis of asteroids in terms of trajectory, shape, composition, morphology, albedo, rotational state, etc., allowing PHAs to be recognized and the probability and timing of a possible collision with Earth to be predicted. This task is mainly carried out thanks to networks that use ground and space telescopes. Pan-STARRS (Panoramic Survey Telescope and Rapid Response System) in the Hawaiian Islands [12] and the LSST (Large Synoptic Survey Telescope) project currently under development in Chilean territory [13] are two terrestrial telescopes used to identify new asteroids.

When an asteroid presents an unacceptable collision risk, or if the uncertainties associated with its trajectory lead to the hypothesis of a possible impact during subsequent resonant encounters with Earth, it is necessary to consider the implementation of strategies aimed at deviating the trajectory of the PHA. Two aspects influence the choice of the strategy to be implemented: the size of the impacting body and the residual time before impact. For bodies in the order of a few meters in diameter, it is generally preferable to evacuate the region where the impact is expected to occur [14]. For larger asteroids, especially those at least 100 m in diameter, and in the case of longer time horizons, more complex mitigation strategies can be considered that can be grouped into two categories: The first category includes those based on impulsive maneuver, where a speed variation is applied, which, although very small compared with the orbital speed, usually in the order of mm/s, allows changes in the trajectory that increase the MOID by a sufficient number of planetary radii to cancel the impact risk. The second category includes those in which the deviation is the result of a force applied on the asteroid that is much smaller than in the impulsive case, but prolonged over an extremely long time period.

Among impulsive variations, at least two approaches can be considered: nuclear deflection, which is limited only to asteroids characterized by large size and/or short action time (shorter than a decade) [15], and kinetic impactor (KI), in the case of diameters in the order of hundreds of meters and with a medium to long time horizon [16–19]. A KI offers the advantage of relying on well-established and relatively simple technologies. It has already been tested by the Deep Impact and DART missions. Deep Impact allowed a 370 kg probe to collide with Comet P/Tempel 1 on 4 July 2005 at a relative velocity of 10.2 km/s [20], whereas DART successfully impacted Dimorphos at approximately 6.15 km/s [21–23], reducing its orbital period around Didymos by more than 30 min ($-33.0 \pm 1.0 (3\sigma)$ min) by virtue of an instantaneous reduction in Dimorphos's along-track orbital velocity component of $-2.70 \pm 0.10\ (1\sigma)$ mm/s [24].

Among nonimpulsive maneuver types, at least three possible strategies should be considered. The gravitational tractor (GT) involves placing a sufficiently large mass in heliocentric orbit near the PHA to perturb its motion enough to change the trajectory and increase the MOID [10,25]. A second possibility is offered by the use of technologies based

on ionic propulsion (ion-beam shepherd); this choice greatly simplifies mission design, but requires a particularly long time horizon for significant changes in the orbit of the asteroid [26,27]. The last and more complex technique is based on artificially induced modification of the albedo coefficient to exploit the Yarkovsky effect [28] to change the trajectory of the asteroid [29]; even in this case, the time horizon must be particularly long to have significant variations in the MOID. In any case, and as will be seen later, the success of a deflection is strongly conditioned by knowledge of the asteroid in all its aspects, such as size, density (porosity), strength, and surface morphology [30–32].

In this paper, the possibility of preventively deviating a body of more than 100 m in diameter with a high risk of collision with Earth will be analyzed using a KI. The object of the deflection is the well-known 2011 AG5 asteroid, with a diameter of about 140 m and identified during the year 2011 (https://minorplanetcenter.net/mpec/K11/K11A31.html, accessed on 12 December 2023). The first observations allowed for an estimate of its orbital parameters, which showed a 17:10 resonance with Earth's orbital period (every 17 Earth revolutions, the asteroid completes 10 revolutions around the Sun). For this asteroid, in the first evaluation, the impact probability was estimated to be $\geq 1/625$ [33] for the second of the two subsequent Earth proximity encounters, scheduled for 2023 and 2040, respectively. Further observations, and in particular those of 2013, allowed for a re-evaluation of its trajectory, ruling out any possibility of a catastrophic event on 5 February 2040. However, the threat posed by this asteroid has been a stimulus to investigate collision mitigation strategies. The paper is structured as follows: Section 2 presents the mathematical model of resonant encounters. Specifically, Section 2.1 introduces Öpik theory, Section 2.2 defines the b-plane, Section 2.3 evaluates the effects of a close encounter of an asteroid with a planet, and Section 2.4 defines the concept of keyhole. In Section 3, the 2011 AG5 asteroid is introduced. Its trajectory is propagated, taking into account updated knowledge of orbital elements, to confirm that there will be no impact in 2040 (Section 3.2). Therefore, the orbital elements are appropriately modified in Section 3.3 to obtain a virtual impactor. Section 4 evaluates the effects of an impulsive deflection with a kinetic impactor. Section 5 presents the results of virtual impactor deflecting maneuvers: the dependence of the deflection on the position in the orbit is evaluated in Section 5.1; the effects of the maneuver epoch are evaluated in Section 5.2, while the effectiveness of the maneuver is investigated as a function of the momentum enhancement factor β in Section 5.3.

2. Resonant Encounters: Mathematical Model

A resonant encounter occurs when the ratio of the orbital period of a small body to that of a planet can be described by integer numbers. In particular, an asteroid is resonant with a planet (e.g., Earth) if, for every h revolution completed by the asteroid, the planet completes k revolutions (resonance $k : h$, with h and k integer numbers). When the semimajor axis of the orbit of the asteroid is greater than that of the planet, then $h < k$; vice versa, $h > k$. The study of bodies with orbits resonant with Earth is central to the identification and monitoring of NEOs.

The study of small bodies' dynamics characterized by resonant orbits with Earth had its beginnings at the end of the 18th century, thanks to theories developed by Anders Johan Lexell (1740–1784) and Urbain Le Verrier (1811–1877). Lexell observed the periodic passages of the comet D/Lexell (D/1770 L1) [34]. Le Verrier, reanalyzing the series of observations of the D/Lexell comet, established that the orbital parameters could not be uniquely determined at a specific epoch, but could be expressed as a function of a single free parameter whose value could vary at ± 1.5 [35].

For a long time, a simplified treatment based on the so-called Line of Variations (LOV) was preferred. Several different definitions of LOV are possible; generally, this approach considers a one-dimensional segment of a curved line—the LOV—in the initial condition space [36].

Ernst Julius Öpik (1893–1985) formulated an original theory of planetary encounter based on a two-body approach. Öpik theory involves evaluating the small body in an

elliptical heliocentric orbit until its distance from another attracting body (e.g., a planet) is small enough to consider the asteroid in the sphere of influence of that body. Then, the orbit of the small body is re-evaluated in a new planetocentric reference frame in which it describes a hyperbolic orbit, treated with a two-body approach [37,38]. A limit of Öpik theory is that it assumes a MOID equal to zero (i.e., the orbit of the small body intersects the target planet). Another limitation is that it neglects the dependence of subsequent asteroid–planet encounters on previous encounters (resonant encounters) [39]. Although implicitly contained in the works of Lexell and Le Verrier, the theory of resonant encounters has only been taken into consideration in recent years [40]. The extension of Öpik theories to encounters with a nonzero MOID, combined with the resonant orbit-based approach, allows for the identification of a region of the b-plane called a keyhole (both described later), such that if the small body passes through it in a close approach, it can lead to a collision with the planet in one of the subsequent resonant encounters [41].

Although, in this work, mitigation strategies will be investigated with numerical simulations, it is useful to present the theoretical elements that allow for the analytical evaluation of impact possibilities for resonant asteroids. Furthermore, the proposed equations are used in Section 3.2 to make the 2011 AG asteroid a virtual impactor (VI). Therefore, in this section, the essential mathematical relationships that describe Öpik theory of close encounters and subsequent extensions for the identification of keyholes in the resonant encounter treatment are provided.

2.1. Öpik Theory

The Öpik resonant encounter theory is based on a two-body model where the attracting body is initially the Sun, and the asteroid moves in an elliptical heliocentric orbit. During a close encounter with a planet, the motion of the small body is considered in a planetocentric reference frame, in which the orbit of the asteroid is hyperbolic. The relative velocity of the small body with respect to the planet allows for the definition of the direction and velocity of the hyperbolic asymptote at entry. These quantities depend solely on the semimajor axis (a), eccentricity (e), and inclination (i) of the heliocentric orbit of the small body. The effect of the encounter is expressed by an instantaneous deviation of the velocity vector in the direction of the outgoing asymptote from the planetocentric orbit, neglecting the perturbing effects of the Sun and other bodies and assuming that the passage occurs instantaneously.

Öpik theory includes some presuppositions. First, the simplifying hypothesis is assumed to be true, that the planet has a circular heliocentric orbit. Moreover, the characteristic quantities are normalized so that the mass of the Sun and the planetary orbit's semimajor axis (a_p) have a unitary value, the orbital period of the planet is 2π, and thus the heliocentric velocity of the planet is unitary. The planetocentric reference frame (X, Y, Z) is defined so that the Y-axis coincides with the direction of the planet's motion, the line connecting the planet and the Sun is along the $-X$ direction, and Z is obtained by the cross product of the other directions, forming a right-handed frame. In this reference frame, the small body's coordinates X_b, Y_b, Z_b—corresponding to the closest undisturbed point—which corresponds to a true anomaly v_b, in the planetocentric reference frame, are given by [42]

$$\begin{bmatrix} X_b \\ Y_b \\ Z_b \end{bmatrix} = \begin{bmatrix} \frac{a(1-e^2)}{(1+e\cos v_b)} - 1 \\ \frac{a(1-e^2)}{(1+e\cos v_b)} \left\{ \Omega + 2\arctan\left[\frac{\sin(\omega+v_b)\cos i}{1+\cos(\omega+v_b)} \right] - \lambda_p \right\} \\ \frac{a(1-e^2)}{(1+e\cos v_b)} \sin i \sin(\omega + v_b) \end{bmatrix}, \quad (1)$$

where ω, Ω, and λ_p are, respectively, the argument of perihelion, the ascending node longitude, and the longitude of the small body. In Equation (1), according to Öpik theory, $a_p = 1$ has been considered.

The components of the unperturbed planetocentric small body velocity vector ($\bar{U}$) are expressed by [43]

$$\bar{U} = \begin{bmatrix} U_x \\ U_y \\ U_z \end{bmatrix} = \begin{bmatrix} \pm\sqrt{2 - \frac{1}{a} - a(1-e^2)} \\ \sqrt{a(1-e^2)}\cos i - 1 \\ \pm\sqrt{a(1-e^2)}\sin i \end{bmatrix} = \begin{bmatrix} U\cos\theta\sin\phi \\ U\cos\theta \\ U\sin\theta\cos\phi \end{bmatrix}. \quad (2)$$

In Equation (2), θ is the angle formed between $\bar{U}$ and the heliocentric velocity of the target planet, while φ is the angle between the plane containing $\bar{U}$ and the heliocentric velocity of the target planet and the ecliptic pole. The norm of $\bar{U}$ is $|\bar{U}| = \sqrt{3 - \frac{1}{a} - 2\sqrt{a(1-e^2)}\cos i} = \sqrt{3-T}$, with T as the Tisserand invariant: $T = \frac{1}{a} + 2\sqrt{a(1-e^2)}\cos i$.

2.2. The b-Plane

The b-plane is defined as the plane orthogonal to the velocity vector $\bar{U}$ and containing the center of the planet [44]. The vector $\bar{b}$ connects the planet to the intersection of the hyperbolic entrance point with the b-plane, and its norm ($b = |\bar{b}|$) is defined as the impact parameter. While the MOID represents the minimum Euclidean distance between two orbits (e.g., the asteroid and Earth), b is the closest distance between the trajectory of the asteroid and the center of the planet on the b-plane. Both $\bar{b}$ and the point with coordinates (X_b, Y_b, Z_b) lie in the b-plane.

Therefore, a new planetocentric coordinate system (ξ, η, ζ) is defined in which ξ and ζ are the coordinates in the b-plane and η is directed along $\bar{U}$. The ζ axis is directed in the opposite direction to the projection onto the b-plane of the planet's heliocentric velocity; finally, the ξ axis, which completes the right-handed triplet, is perpendicular to the planet's heliocentric velocity. In this way, the minimum distance between the planetocentric orbit and the planet, constructed along the ξ axis, can be identified: this is the MOID. Similarly, the ζ axis can be seen as a time coordinated [39]. The use of these two coordinates (ξ, ζ) allows for the decoupling of the two parameters that control the possibility of a close encounter, the distance between the orbits (ξ) and the encounter moment (ζ). These two parameters can be controlled only by two heliocentric orbital elements: the mean anomaly (M) and the argument of perihelion (ω).

In the new reference coordinate system (ξ, ζ), the position of the small body can be described using the initial conditions (X_b, Y_b, Z_b) and the angles θ and ϕ [42]:

$$\xi = X_b\cos\phi - Z_b\sin\phi; \quad (3)$$

$$\zeta = (X_b\sin\phi + Z_b\cos\phi)\cos\theta - Y_b\sin\theta. \quad (4)$$

2.3. Close Encounter

An interplanetary encounter results in a rotation of the velocity vector $\bar{U}$ of the small body, with no associated changes in its magnitude. Therefore, the pre-encounter angles θ and ϕ change to the postencounter values θ' and ϕ', whereas the postencounter orbital elements are a', e', and i'. The equations that define the postencounter parameters are proposed in [42,45]. An explicit expression of the postencounter MOID (as a function of the previous one) is given by

$$\xi' = \frac{(b^2 + c^2)\xi\sin\theta}{\sqrt{[(b^2 - c^2)\sin\theta - 2c\zeta\cos\theta]^2 + 4c^2\xi^2}}, \quad (5)$$

where $c = m/U^2$, with m as the mass of the planet normalized with respect to the mass of the Sun, and $b^2 = \xi^2 + \zeta^2$. The new MOID cannot be zero if $\sin\theta \neq 0$ (except when the previous MOID was zero, $\xi = 0$).

Although the theory of Öpik presents limitations of applicability both in the case of exactly tangent and coplanar orbits and in the more general case $\sin\theta \simeq 0$ [44], it constitutes a valid analytical alternative to numerical integrations. The great advantage provided by this theory, particularly evident for resonant encounters, is that of being able to estimate in an extremely rapid manner the subsequent positions in the b-plane of the small body, allowing for evaluating the MOID of the subsequent encounters.

2.4. Keyhole

A keyhole refers to small regions in the b-plane such that if an asteroid passes through one of them in a resonant encounter, it will hit the planet in the next encounter, or more generally, it will pass very close to the planet [41]. The keyhole is just one of the possible pre-images of the Earth cross section on the b-plane, related to the value of the postencounter semimajor axis (a'). It is necessary to take into account secular perturbative effects that act on long timescales and short-period effects related, for example, to third-body perturbations, which produce MOID variations [46].

In order to derive the MOID of the next encounter (ξ'') from the previous one (ξ' defined in Equation (5)), the temporal variation of ξ has been linearized as follows [39]:

$$\xi'' = \xi' + \frac{d\xi}{dt}(t_0'' - t_0'); \tag{6}$$

where t_0'' and t_0' denote the times of the initial passage at the node during the second and first encounters, respectively. The accurate calculation of $d\xi/dt$ is particularly challenging and can be carried out using numerical integrations to limit errors in the estimation of the MOID of the next encounter.

The Earth impact cross section (b_E) is defined as

$$b_E = r_E\sqrt{1 + \frac{V_E^2}{U^2}}; \tag{7}$$

with r_E as the (mean) planetary radius of Earth and $V_E^2 = 2\mu_E/r_E$ as the Earth escape velocity (μ_E is the gravitational parameter of Earth). As is evident in Equation (7), $b_E > r_E$, while the impact occurs when $b \leq b_E$. The keyhole is defined by the pairs of points (ξ', ζ') related to the first encounter that, as a result of Keplerian propagation and taking into account the previously defined variation of the MOID, produce pairs of points (ξ'', ζ'') that fall within a circle centered at the origin and radius b_E.

To define the shape and size of the keyhole, it is possible to consider the partial derivative matrix, valid when $c^2 \ll b^2$:

$$\begin{bmatrix} \frac{\partial\xi''}{\partial\xi} & \frac{\partial\xi''}{\partial\zeta} \\ \frac{\partial\zeta''}{\partial\xi} & \frac{\partial\zeta''}{\partial\zeta} \end{bmatrix} \approx \begin{bmatrix} 1 + o(\frac{c}{b}) & o(\frac{c}{b}) \\ o(1) - \frac{2hf\xi\zeta}{b^4} & 1 + o(\frac{c}{b}) + \frac{hf(\xi^2-\zeta^2)}{b^4} \end{bmatrix}. \tag{8}$$

In Equation (8), f is a constant that does not depend on h (heliocentric revolutions of the asteroid between the two resonant encounters). Although MOID remains largely unchanged, ζ'' varies linearly with h. Moreover, except for the case where $\xi \approx \zeta$, $\partial\zeta''/\partial\zeta$ can generally be quite large; in terms of pre-image, this translates into a crescent-shaped keyhole closely following the circumference on the b-plane and having a thickness along the ξ axis of approximately $2b_E$ and a maximum thickness of $\sim[2b_E/(\partial\zeta''/\partial\zeta)]$. When $\xi = \zeta$, $\partial\zeta''/\partial\zeta$ can also be less than 1, which can imply a keyhole whose size in ζ is larger than b_E.

3. Virtual Impactor Based on the Asteroid 2011 AG5

The long-term propagation of the trajectory of the asteroid 2011 AG5, taking into account the current knowledge of its orbital elements and their uncertainties, ruled out any possibility of impact in upcoming resonant encounters. However, by appropriately

modifying some orbital elements (argument of perihelion and true/mean anomaly), it can be transformed into a VI, an asteroid that can hit Earth (or pass extremely close) in one of its resonant encounters. Once a VI is realized, the trajectory deflection maneuvers based on a KI will be proposed.

This section describes the characteristics of the asteroid 2011 AG5 and the procedure for creating a VI.

3.1. The Asteroid 2011 AG5

The 2011 AG5 asteroid was cataloged in early 2011 (Minor Planet Electronic Circular (MPEC) 2011-A31) (https://minorplanetcenter.net/mpec/K11/K11A31.html, accessed on 12 December 2023). The observations that took place during 2011 (up to September) allowed an initial estimate of the orbital and physical characteristics and uncertainties. The first long-term propagation showed that the orbit of the asteroid, characterized by a 17:10 resonance with Earth, had a probability of impact $\geq 1/625$ for the encounter on 5 February 2040. A critical role would have been played by the close encounter in February 2023, at an estimated distance of 0.0123 astronomical units, during which the asteroid could have potentially passed through a keyhole with a width of 365 km. Since NASA Jet Propulsion Lab's (JPL) NEO Program (https://neo.ssa.esa.int/search-for-asteroids?tab=summary&des=367789%202011AG5; last access: 12 December 2023) estimated the diameter, apparent magnitude, and mass of the asteroid to be ∼150 m, H = 21.8 mag, and 4.0×10^9 kg, the possibility that 2011 AG5 could impact Earth generated great interest in the scientific community.

October 2013 observations, when the position of 2011 AG5 in opposition to the Sun and near Earth allowed more accurate orbital elements, excluded any possibility of impact in 2040 [33].

Therefore, it was necessary to characterize the asteroid with greater accuracy in order to reduce the uncertainty of the trajectory from ∼400 Earth planetary radii to no more than 2.

Subsequently, other observations, particularly those of November 2015 and September 2018 favored by a solar elongation angle close to 180 deg, allowed for a more complete definition of the orbital parameters. The values estimated by NEODyS on 9 October 2018, which have been considered in this work, are reported in Table 1.

Table 1. Orbital elements of the asteroid 2011 AG5 on 9 October 2018 (computed by NEODyS and taken from https://neo.ssa.esa.int/search-for-asteroids?tab=orbprop&des=367789%202011AG5; last access: 12 December 2023). These orbital elements, along with their uncertainties, yield no possibility of collision with Earth.

	Reference Value	**Standard Deviation (σ)**
Epoch	**9 October 2018**	
a (AU)	1.430783	3.666×10^{-8}
e	0.390271	3.568×10^{-8}
i (deg)	3.682	6.656×10^{-6}
Ω (deg)	135.667	4.541×10^{-5}
ω (deg)	53.558	4.593×10^{-5}
M (deg)	147.036	6.023×10^{-5}

3.2. Trajectory Propagation

For the propagation of the asteroid trajectory, the J2z000 ecliptic heliocentric inertial coordinated reference system has been adopted. In this reference frame, the xy plane is defined by the ecliptic plane (i.e., the orbital plane of Earth's motion around the Sun), fixed on 1 January 2000 at 12:00 p.m. The x-axis is directed towards the first Aries point; the y-axis is defined orthogonally to the x-axis in the ecliptic plane. Finally, the z-axis is normal to the xy plane to complete the right-handed coordinate system.

The orbit of the asteroid 2011 AG5 has been propagated using a numerical integrator. The attraction of the Sun and the other main bodies (Venus, the Earth–Moon system, Mars, and Jupiter) has been taken into account. The initial conditions of the asteroid are obtained from the average orbital elements provided by the NEODyS website on 58,400.0 MJD (9 October 2018 at 0:00), as reported in Table 1. The equations of motion are solved using the MATLAB ODE113 numerical integrator (https://www.mathworks.com/help/matlab/ref/ode113.html; last access: 12 December 2023). For the trajectories of other bodies (Earth–Moon, Jupiter, Mars, and Venus), the DE430 planetary and lunar ephemerides have been considered [47]. In Figure 1A, the 3D trajectories of the asteroid 2011 AG5 (purple line), Earth (blue), and Mars (green) are represented; Figure 1B shows the projections of the same curves in the xy ecliptic plane. These figures highlight the evolution of the asteroid heliocentric orbit, from October 2018 to February 2040, due to the perturbative effects of the other planets in the Solar System and, in particular, the close encounter with Earth in February 2023. Note that, in Figure 1A,B and in all subsequent figures related to the trajectories of propagated bodies, a color scheme similar to the NEOShield study report [48] has been adopted (with purple instead of red); in this way, the graphs of the present work are easily comparable with those of the aforementioned work. Figures 2 and 3 show the two asteroid passages near Earth, respectively, in 2023 and 2040. Figure 2 shows the projection of the trajectory of 2011 AG5 onto the ecliptic plane relative to Earth, reported in a geocentric-ecliptic reference (whose axes coincide with the reference described above, but the origin is translated to the center of Earth). This graph shows how, using orbital elements known as of 2018, the first of two passages in February 2023 is characterized by a MOID, quantified in the subsequent Figure 3, at 0.0113 AU. The latter plot, showing the temporal evolution of the relative distances between the asteroid and the Sun (blue line), Earth (purple), and Mars (green), allows for an estimate of the MOID in the expected passage for 2040 $\simeq$ 0.052 AU.

(**A**)

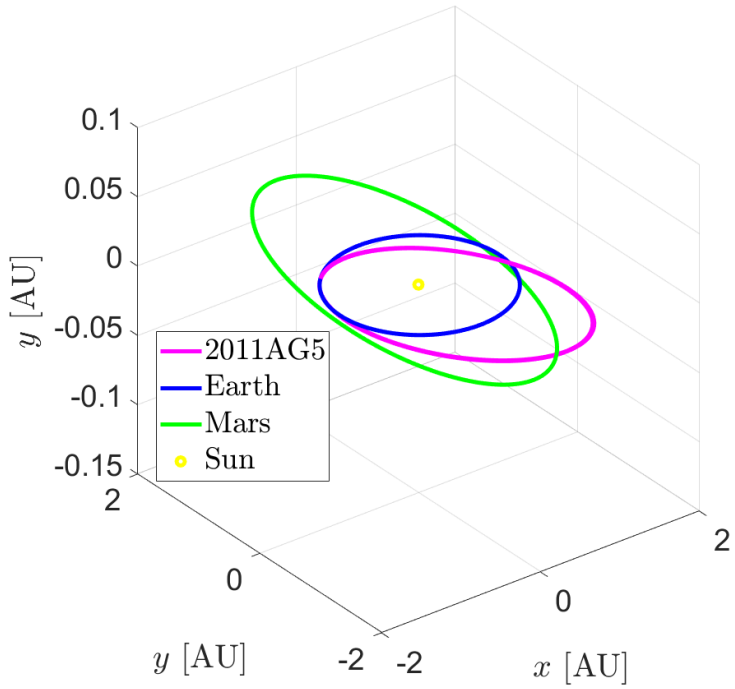

Figure 1. *Cont.*

(**B**)

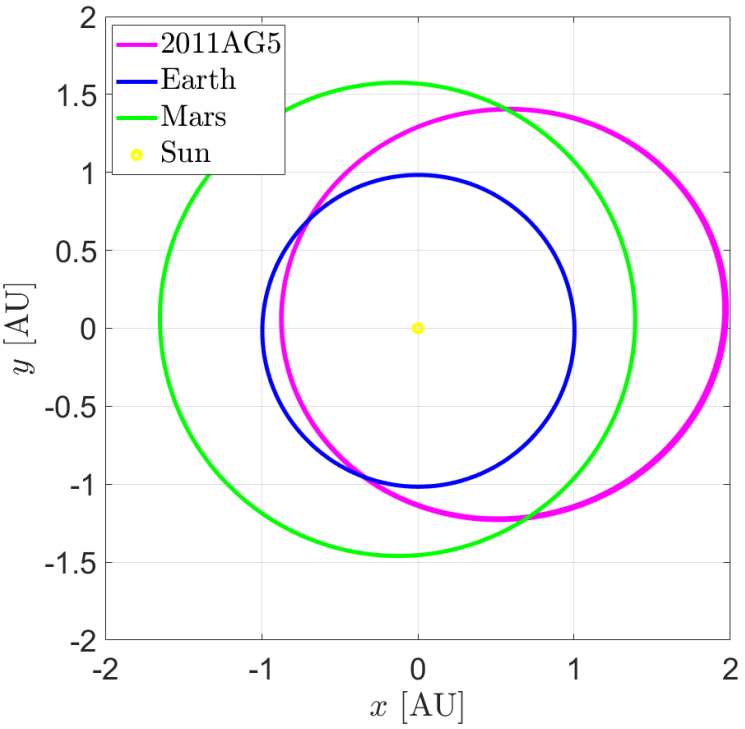

Figure 1. (**A**) 3D real trajectories (i.e., considering orbital elements in Table 1) of 2011 AG5 (purple line), Earth (blue), and Mars (green) between 9 October 2018 and 15 June 2040. (**B**) Their projection onto the ecliptic plane.

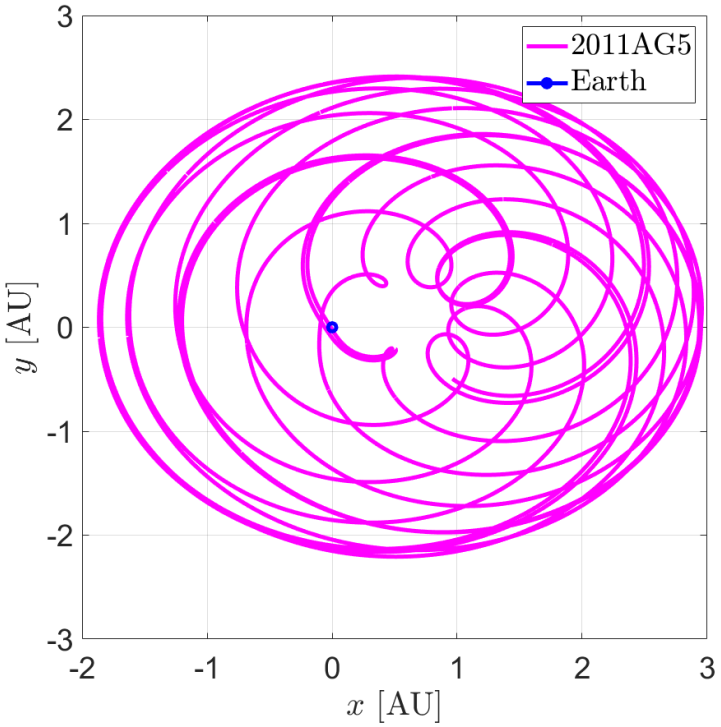

Figure 2. Projection of the real relative trajectory (i.e., considering orbital elements in Table 1) with respect to Earth of the 2011 AG5 asteroid onto the ecliptic plane in a geocentric-ecliptic reference frame.

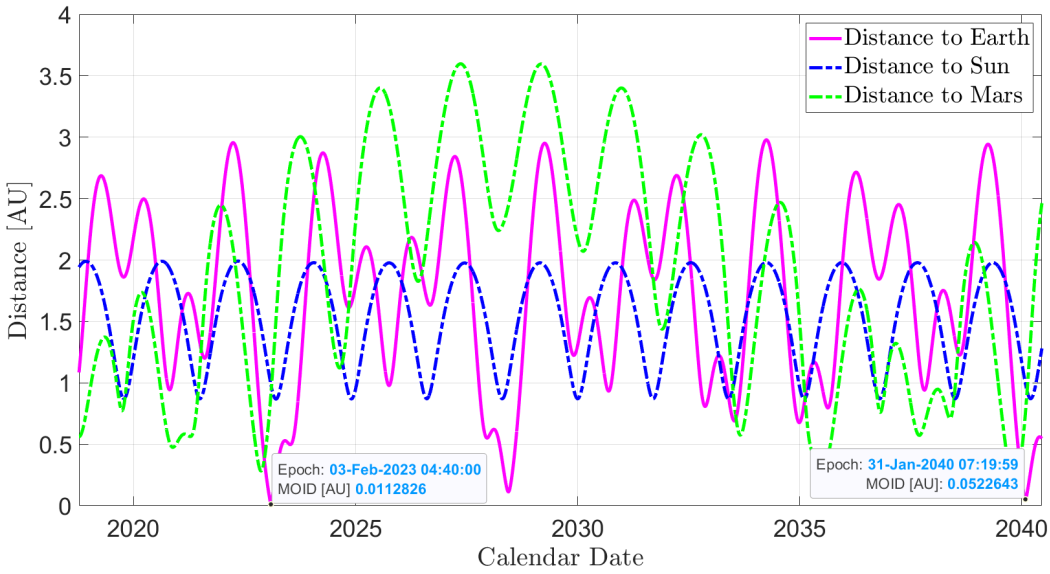

Figure 3. Evolution of the relative real distances (i.e., considering orbital elements in Table 1) between the 2011 AG5 asteroid and the Sun (blue line), Earth (purple), and Mars (green). Data tips report the MOID in the close encounter in 2023 and 2040.

Since these results rule out the possibility of a collision, the values in Table 1 have been modified to make a 2011 AG5 VI. Later, suitable deflective maneuvers to avoid impact in February 2040 will be proposed.

3.3. The Virtual Impactor

To test the effects of a preventive corrective maneuver on an asteroid, the orbital elements (in Table 1) have been modified to have a MOID lower than b_E (see Equation (7)) in encounters in 2040. In this way, the asteroid becomes a VI.

In the b-plane, the collision depends on the two coordinates ξ and ζ. They are a function of ω and λ_p, or better of $M - \lambda_p$. Assuming small initial values of the coordinates in the b-plane ($\xi \approx 0$ and $\zeta \approx 0$), it is possible to evaluate the effects that, when other orbital elements are constant, small variations $\delta\omega$ and $\delta\lambda_p$ induce in ξ and ζ following the procedure described in [42]. First, the following partial derivatives have to be computed:

$$\frac{d\xi}{d\omega} = -\frac{U \sin\theta \sin\varphi \cos\varphi}{\sqrt{(1 + U\cos\theta)^2 + U^2 \sin^2\theta \cos^2\varphi}}; \tag{9}$$

$$\frac{d\zeta}{d\omega} = -\frac{\sin\theta\left(1 + U\cos\theta \sin^2\varphi\right)}{\sqrt{(1 + U\cos\theta)^2 + U^2 \sin^2\theta \cos^2\varphi}}; \tag{10}$$

$$\frac{d\xi}{d\lambda_p} = 0; \tag{11}$$

$$\frac{d\zeta}{d\lambda_p} = -\sin\theta. \tag{12}$$

Using Equations (9)–(12), the equations that connect the small displacements $\delta\omega$ and $\delta\lambda_p$ to the variations they produce in ξ and ζ can be linearized as follows:

$$\begin{bmatrix} \xi \\ \zeta \end{bmatrix} = \begin{bmatrix} \frac{\partial\xi}{\partial\omega} & \frac{\partial\xi}{\partial\lambda_p} \\ \frac{\partial\zeta}{\partial\omega} & \frac{\partial\zeta}{\partial\lambda_p} \end{bmatrix} \begin{bmatrix} \delta\omega \\ \delta\lambda_p \end{bmatrix} \tag{13}$$

To generate the VI, it is sufficient to modify only the orbital elements involved in Equation (13): ω and, as a counterpart of λ_p, M (which depends on λ_p). Table 2 shows the modified orbital elements of the VI: a comparison with those in Table 1 shows that the variation of $\delta\omega$ is in the order of 10^{-4} deg, while the displacement δM is in the order of 10^{-2} deg (about 0.03 deg); the correction δM is greater because M has a more substantial influence on the timing of the encounter. The identified VI is just one of the possible scenarios. For a pair of correction values $(\delta\omega, \delta M)$ to lead to a VI, it must be such that it guides the asteroid through the keyhole associated with the close passage in February 2040.

Table 2. Orbital elements of the asteroid 2011 AG5 modified to have a VI.

	Reference Value
Epoch	**9 October 2018**
a (AU)	1.43078
e	0.390271
i (deg)	3.682
Ω (deg)	135.667
ω (deg)	53.5579955
M (deg)	147.069699

Figure 4 shows the relative distances between the VI and the other celestial bodies considered; the purple line, related to the asteroid–Earth distance, shows how, with modified orbital elements, the asteroid hits Earth in 2040.

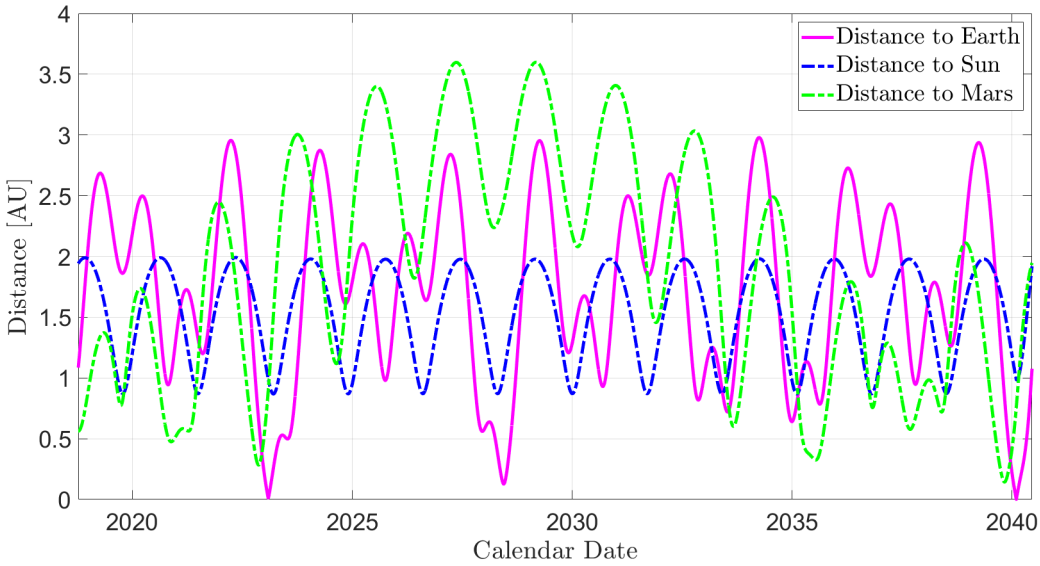

Figure 4. Evolution of the relative distances between the VI (based on the 2011 AG5 asteroid) and the Sun (blue line), Earth (purple), and Mars (green).

4. Kinetic Impactor

In this section, the equations that describe the effects of an asteroid deflecting maneuver with a KI are presented. The deviation can be synthesized by an impulsive maneuver that induces a change in the momentum of the asteroid. Part of the change in momentum is due to the high-speed collision between the spacecraft (the impactor) and the NEO. An additional contribution to Δv is offered, according to the principle of action and reaction, by the materials ejected outward from the crater generated during the impact. The velocity variation is described by the following equation [7,49]:

$$\Delta v = \beta \frac{m_{sc}}{m_a} \Delta V_t^{sc}, \tag{14}$$

where m_{sc} is the mass of the spacecraft at impact, m_a the mass of the asteroid, ΔV_t^{sc} the projection of the spacecraft/asteroid relative velocity along the direction of the velocity of the asteroid (tangential direction), and β the multiplicative factor of momentum, a coefficient that takes into account the mass ejection that follows the collision. This coefficient makes it possible to quantify the component of the total change in the asteroid momentum as a multiple of the component of this change resulting from the collision. In fact, using Equation (14), the scalar change in the momentum of the impacted body can be written as follows:

$$\Delta p = m_a \Delta v = \beta m_{sc} \Delta V_t^{sc} = (\beta - 1) m_{sc} \Delta V_t^{sc} + m_{sc} \Delta V_t^{sc} \tag{15}$$

where the component due to the high-speed mass ejection can be distinguished from that due to the collision. The coefficient β represents a source of uncertainty in the effects of the maneuver, as it can be estimated experimentally or by numerical simulations, provided that the characteristics of the internal structure and the morphological characteristics of the asteroid are accurately known. The methodology for determining the coefficient has been widely analyzed in the literature [50,51]. Equation (14) shows how maneuver effects depend linearly on ΔV_t^{sc}, so it is necessary to consider the technological limits on the spacecraft/asteroid relative speeds that are feasible. In addition to the limits of the launcher, which also depend on the approach orbit, those related to the GNC (guidance, navigation, and control) system during rendezvous with an object whose diameter is in the order of 100–150 m must also be considered. In a similar scenario, the limit values for ΔV_t^{sc} are indicated in the literature to be up to 15 km/s [52]. Furthermore, since ΔV_t^{sc} is the projection of the relative velocity along the asteroid direction, it will depend on the angle of incidence (α) of the spacecraft speed at impact. Thus, given the spacecraft velocity vector $\bar{v}_{sc}$ (with $v_{sc} = |\bar{v}_{sc}|$ its module) and the minimum change in the asteroid velocity vector that can guarantee a sufficient deviation to avoid the risk of collision with the planet ($\Delta \bar{v}_{req}$), the constraints to be placed on the spacecraft/asteroid impact angle that the GNC system must guarantee are defined by the following equation:

$$\Delta v = \frac{\Delta \bar{v}_{req}}{\cos \alpha} \frac{\bar{v}_{sc}}{v_{sc}}. \tag{16}$$

By decomposing the vector $\Delta \bar{v}$ into its three components—tangential, normal, and outside the orbital plane ($\Delta \bar{v} = \begin{bmatrix} \delta v_t & \delta v_n & \delta v_h \end{bmatrix}^T$)—the variation of the orbital elements due to $\Delta \bar{v}$ is given by [17]

$$\delta a = \frac{2a^2 V}{\mu} \delta v_t \tag{17}$$

$$\delta e = \frac{1}{V} \left[2(e + \cos v_d) \delta v_t - \frac{r}{a} \sin v_d \delta v_h \right] \tag{18}$$

$$\delta i = \frac{r \cos \varpi d}{H} \delta v_h \tag{19}$$

$$\delta \Omega = \frac{r \sin \varpi_d}{H \sin i} \delta v_h \tag{20}$$

$$\delta \omega = \frac{1}{eV} \left[2 \sin v_d \delta v_t + \left(2e + \frac{r}{a} \cos v_d \right) \delta v_n \right] - \frac{r \sin \varpi_d \cos i}{H \sin i} \delta v_h \tag{21}$$

$$\delta M = -\frac{b}{eaV} \left[2 \left(1 + \frac{e^2 r}{p} \right) \sin v_d \delta v_t + \frac{r}{a} \cos v_d \delta v_n \right], \tag{22}$$

in which $p = a(1 - e^2)$ is the semilatus rectum, $H = \sqrt{\mu p}$ is the angular momentum, $r = p/(1 + e \cos v)$ is the orbital radius (v is the true anomaly), V is the module of the orbital velocity of the asteroid ($\bar{V}$) at the moment of deviation, and $\varpi_d = v_d + \omega$ is the argument of latitude of the asteroid at maneuver. In Equation (22), the term δM_n, which

is time dependent, has to be added. This term is due to the change in mean motion ($n = \sqrt{\mu/a^3}$) caused by the variation of the semimajor axis (δa) and is given by

$$\delta M_n = \frac{3}{2}\frac{\sqrt{\mu}\Delta t}{a^{\frac{5}{2}}}\delta a, \tag{23}$$

where Δt is the time elapsed since the maneuver.

Equation (17) highlights that the variation in the semimajor axis is linearly dependent on V and δv_t. Since δa is primarily responsible for variations in MOID and encounter time (δv_t causes a modification of the orbital period), it follows that the most effective maneuvers are those in which the impact occurs at perihelion, where the velocity is maximum, and with $\Delta\bar{v}$ such that δv_t is dominant with respect to other components. Maneuvers performed outside the orbital plane ($\delta v_h \neq 0$) have low efficiency, as they primarily produce $\delta\Omega$ and δi that have a low impact on MOID.

The possibility of deflecting the virtual impactor is investigated in Section 5.

5. Deflection with Kinetic Impactor

In this section, the results of a VI deviation maneuver with a KI are presented. The parameter considered to estimate the effectiveness of the maneuver is the variation of the impact parameter (b). Taking into account the VI in Section 3.3, the goal of this investigation is to modify its trajectory to avoid collision in the resonant encounter in February 2040. The propagation of the trajectory of the asteroid is carried out using the parameters listed in Table 2.

The results obtained in previous works published by the JPL NEO Program Office [33] and Elecnor Deimos for NEOShield [7,48], which present various KI-based deflection campaign hypotheses for the asteroid 2011 AG5, are considered. As indicated by Equations (17)–(22), the impulsive maneuver is more efficient, in terms of δa, if it is performed at the perihelion of the asteroid, imparting $\Delta\bar{v}$ in the direction tangent to the trajectory ($|\Delta\bar{v}| \approx \delta v_t$). For this reason, the dates of subsequent perihelion and aphelion passages after the reference date of the orbital elements (9 October 2018) and prior to the February 2023 (as shown in Figure 3, this is the epoch of the closest and most influential encounter with Earth preceding the potential impact date in 2040) resonant passage are identified, as maneuvers carried out prior to the proximity passage produce greater effects [7,33]. Table 3 lists the aphelion and perihelion epochs between 9 October 2018 and the end of 2024, which will be taken into account for the implementation of corrective maneuvers.

Table 3. Passages of the asteroid 2011 AG5 (VI) at aphelion and perihelion with time to impact. The column 'To Impact' indicates the distance, expressed in years, before the date of the possible collision (5 February 2040).

Position Epoch	I Passage Epoch	To Impact	II Passage Epoch	To Impact
Aphelion	5 December 2018 04:00	21.170 years	21 August 2020 07:00	19.458 years
Perihelion	13 October 2019 17:00	20.313 years	30 June 2021 02:00	18.601 years
Position Epoch	**III Passage Epoch**	**To Impact**	**IV Passage Epoch**	**To Impact**
Aphelion	8 May 2022 02:00	17.747 years	21 January 2024 13:00	16.040 years
Perihelion	16 March 2023 21:00	16.809 years	27 November 2024 06:00	15.189 years

The comparison will first be made between the effectiveness of a maneuver performed at perihelion and that of a correction at aphelion. Subsequently, the influence of the maneuver epoch will be analyzed (by fixing the position of the asteroid along its heliocentric orbit). Later, assuming a scenario similar to that of the Deep Impact and DART missions [53,54], the influence of the factor β will be analyzed.

To evaluate the effects of an impulsive maneuver based on a KI, it is necessary to define the parameters involved in Equation (14). For the mass of the asteroid, the most conservative value $m_a = 4 \times 10^9$ kg has been considered, while m_{sc} is varied, in 100 kg steps, between 100 and 1700 kg, a limit value indicated in the literature [33]. For V_t^{sc}, values between 1 and 15 km/s with a step of 1 km/s are considered. This upper value represents a technological limit related to the performance of the launcher and GNC system [7]. For β, a conservative value of 2 has been assumed (see Section 5.3 for more details); this value has been assumed as a constant, although β is a complicated time-dependent function influenced by multiple factors, including surface geology, topography, and properties of asteroid material [32,55,56]. Finally, Δv is considered to agree or not with the speed of the asteroid, producing its acceleration or deceleration. As a convention, from now on, we will refer to positive Δv (or $\Delta v > 0$) in the first case, while we will refer to negative Δv (or $\Delta v < 0$) for those that cause a deceleration of the asteroid. In Figure 5, the absolute values of Δv, expressed in cm/s, obtained as a function of m_{sc} and V_t^{sc} are reported on a chromatic scale: the characteristic values are in the order of mm/s with a maximum close to 1.2 cm/s.

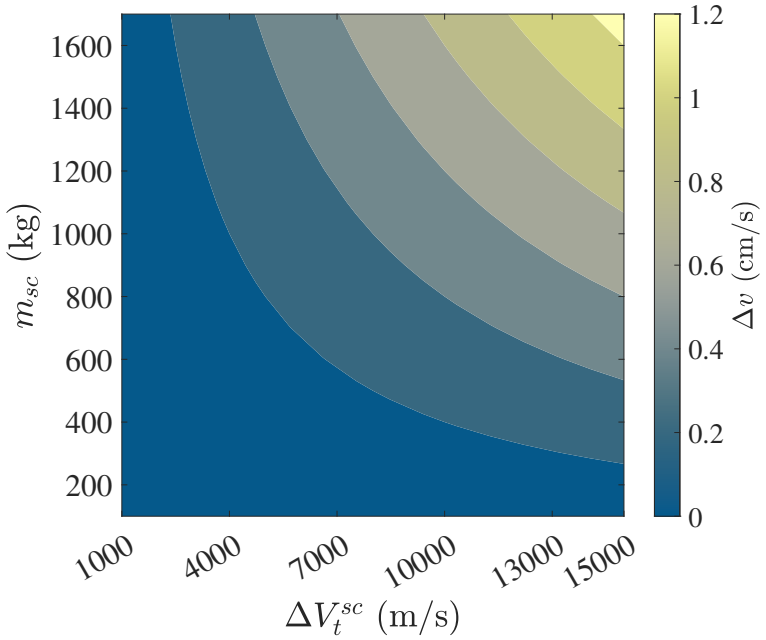

Figure 5. Color plot of Δv (cm/s) as a function of the spacecraft mass and the relative velocity between the asteroid and S/C. Results obtained assuming a constant value for the parameter $\beta = 2$.

5.1. Position on the Orbit

In Figure 6, the deflections are compared, in terms of the variation of b at the resonant passage in February 2040 as a multiple of Earth's planetary radius, for an impulsive maneuver performed at the first perihelion pass on 13 October 2019. The left panel refers to positive Δv, while the right panel refers to negative Δv. In the figures, a saturation value of 12 planetary radii is assumed. This choice is made to improve the readability of the figures; in fact, considering Equation (7), even for low values of U, b_E does not exceed the value of $6r_E$. However, it should be noted that in the saturated region of the graphs (dark blue area), the variation of b can be much greater than 12 Earth radii. Positive Δv induces more significant changes in b. In fact, when $\delta V_t > 0$, an increase in a occurs, whose effects on the change in mean motion are more pronounced than those obtained when $\delta V_t < 0$. Therefore, the maneuvers vary the semimajor axis, then the mean motion, and finally the mean anomaly. In the b-plane, this translates into both a removal of the asteroid's trajectory from the target planet ($\Delta\xi$) and a delay/advance in the encounter timing ($\Delta\zeta$).

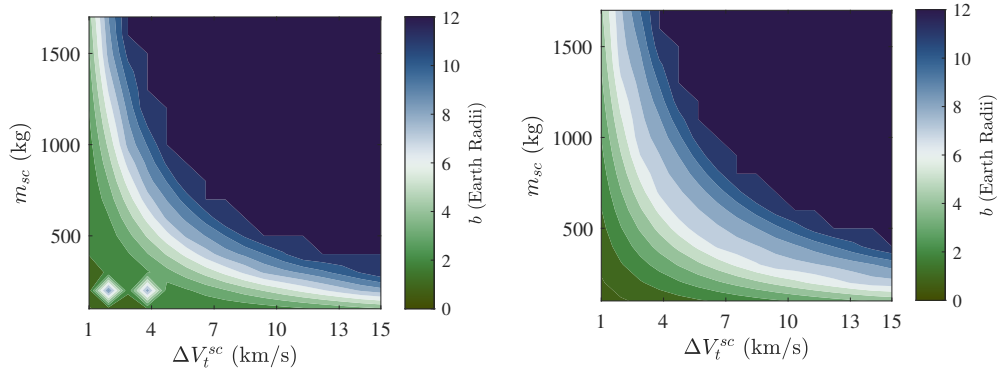

Figure 6. Comparison between positive Δv (**left**) and negative Δv (**right**) for maneuvers performed at the perihelion passage on 13 October 2019. The color scale indicates the variation of b, expressed in Earth radii, with a saturation value of 12. Results obtained assuming a constant value for the parameter $\beta = 2$.

Figure 7 shows the effects of a maneuver at aphelion on 5 December 2018. The graph shows how the contour lines increase and the saturation area (in dark blue) narrows dramatically. Although the maneuver is performed in advance with respect to Figure 6, it produces less significant effects because, at the same Δv, the variation that the impulse produces on a is directly proportional to V at the time of the maneuver (see Equation (17)), which is minimum at aphelion.

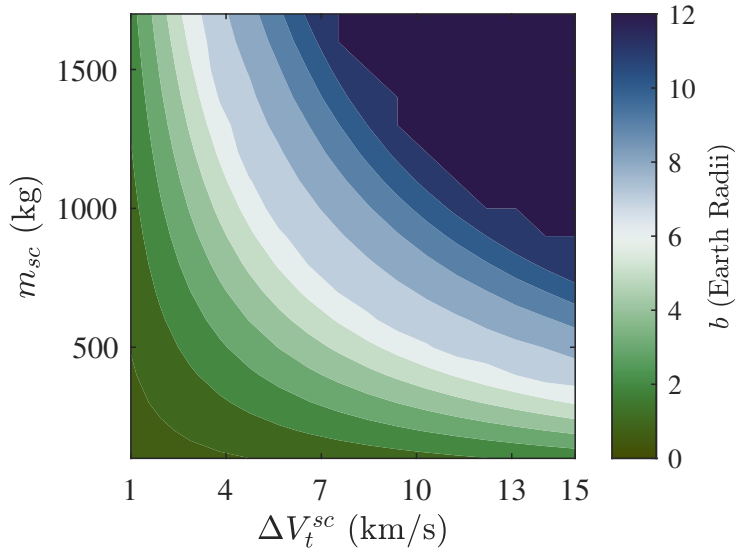

Figure 7. Effects of a maneuver with positive Δv executed at the aphelion passage on 5 December 2018. The color scale indicates the variation of b, expressed in Earth radii, with a saturation value of 12. Results obtained assuming a constant value for the parameter $\beta = 2$.

Assuming for 2011 AG5 a KI similar to that of the Deep Impact mission on Comet Tempel 1, characterized by $V_t^{sc} = 10.3$ km/s and $m_{sc} = 370$ kg [57], comparing Figure 6 and Figure 7, it is evident that the deflection at perihelion (∼21.170 years before the potential impact) would produce a deviation from the target planet of about 10 planetary radii for positive Δv and about 8 planetary radii for positive Δv, while maneuvering at aphelion (∼20.13 years before the potential impact), a deviation of just 3–5 planetary radii would be obtained. Taking into account the characteristics of the DART mission KI [22] ($V_t^{sc} \approx 7$ km/s; $m_{sc} \approx 370$ kg), even the perihelion impact would not guarantee sufficient margins of reliability to avoid collision in 2040, taking into account the uncertainties on the

parameters that influence the exact reconstruction of the maneuver and trajectory, and in particular those related to the knowledge of

- Predeflection orbital elements (mitigable over time with subsequent observations);
- The size of the asteroid;
- The shape of the asteroid;
- The density and mass of the asteroid;
- The albedo coefficient, whose accurate knowledge allows for an estimate of the perturbations due to the Yarkovsky effect; and
- The momentum enhancement factor β.

As stated above, to avoid overestimating the deflection obtained with the maneuvers, a particularly conservative scenario is chosen for both the mass of the asteroid, selecting the largest among the different estimates, and the momentum enhancement factor, whose influence is referred to in Section 5.3, set conservatively at 2.

5.2. Epoch Influence

To assess the influence of the epoch, it is assumed that a maneuver is performed in the next perihelion passage after that in Section 5.1 (plots in Figure 6), on 30 June 2021 (∼18.601 years before the potential impact). The right panel in Figure 8 reports the deflection obtained with a positive Δv; as is evident, the dark blue portion is significantly reduced relative to the left panel in Figure 6, and also with respect to Figure 7. Differences between the deflection achievable by performing the maneuver with positive Δv at the perihelion of 13 October 2019 and those obtained by performing a similar maneuver at the perihelion of 30 June 2021 are represented in the right panel in Figure 8 (this time, the color bar is not saturated). The advantage of maneuvering 2 years earlier is verified for all $\Delta V_t^{sc}/m_{sc}$ pairs, with differences of up to 25 planetary radii under the assumption of the maximum mass of the spacecraft and the relative velocity.

Similar results are found both by considering the perihelion maneuver with negative Δv (as occurred in the DART mission [22]) and in the case of two successive maneuvers at aphelion, that is, by comparing the results of Figure 7 with those of a deflection at aphelion on 21 August 2020.

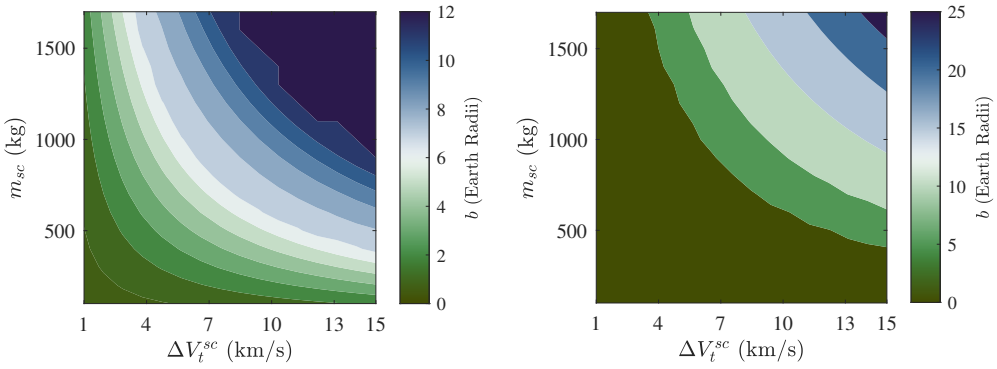

Figure 8. Left panel: effects of a maneuver with positive Δv executed at the perihelion passage on 30 June 2021. The color scale indicates the variation of b, expressed in Earth radii, with a saturation value of 12. Right panel: comparison between the deflection achievable by performing the maneuver at perihelion on 13 October 2019 and those obtained by performing the maneuver at perihelion on 30 June 2021. The color scale indicates the differences in the achievable variation of b, expressed in Earth radii (i.e., the difference in b variation obtained by performing the maneuver on 13 October 2019, minus the variation of b obtained by performing the maneuver on 30 June 2021).

The performance of the maneuver decreases significantly when it is performed after the 2023 resonant encounter. To this end, a mission scenario is considered in which Δv is applied at the next perihelion passage after the resonant encounter in 2023, on 27 November 2024. Figure 9, which refers to a maneuver performed with positive Δv, clearly shows that

if the correction is performed after the resonant encounter in 2023, the maneuver would be effective (changes in b above 10 Earth radii) only for $m_{sc}/\Delta V_t^{sc}$ combinations at the border of technological limits.

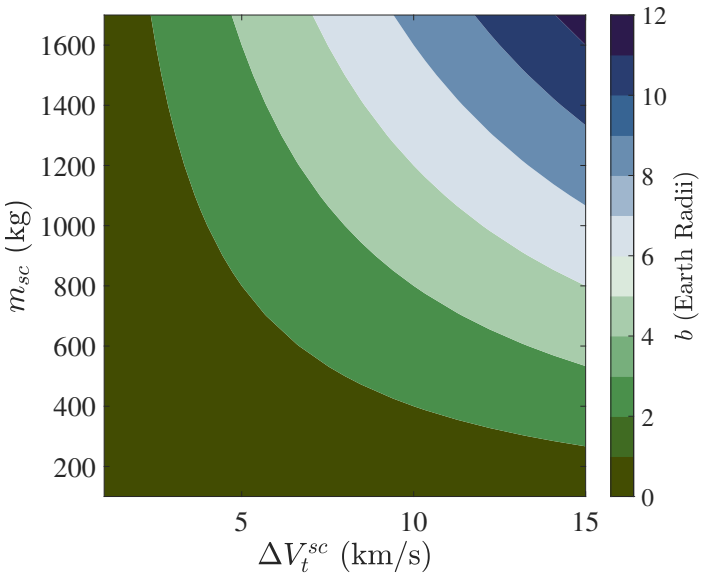

Figure 9. Effects of a maneuver with positive Δv executed at the perihelion passage on 27 November 2024. The color scale indicates the variation of b, expressed in Earth radii, with a saturation value of 12.

5.3. Influence of β

The final investigation focused on the influence of the momentum enhancement factor β. The coefficient β depends on various characteristics of the asteroid, such as porosity, cohesion, morphology, and shape [19]. An influence on β, less than 2%, is also due to the rotational state of the asteroid [30]. Experimental and numerical simulations show characteristic values of β ranging from 1 to 6 [19].

For the present analysis, two real mission scenarios, the Deep Impact and DART missions, have been considered: the real values of the impactors from these two missions (spacecraft mass and relative impact velocity) have been taken into account to perform a deflection maneuver in our scenario, related to the VI based on 2011 AG5. Figure 10 shows the achievable deviations, expressed in Earth's planetary radii, as a function of β, assuming ΔV at the perihelion passage of 13 October 2019 and—as mentioned—adopting the parameters of the Deep Impact and DART missions for the KI (the values have been reported in the legend of Figure 10). The left panel in Figure 10 refers to $\Delta v > 0$, while the right panel refers to $\Delta v < 0$ (real scenario for the DART mission). Since the product of the impactor mass and impact velocity (which linearly influences Δv) is very similar for both missions, the two curves are very close to each other. Figures indicate that the linear dependence of Δv on β produces quasi-linear effects on the variation of b (the maneuver linearly impacts the change in semimajor axis, but nonlinearly affects the change in mean motion, and consequently the mean anomaly). Assuming the deflections for which $b > 10$ Earth radii to be effective, both a KI with the characteristics of the Deep Impact mission (blue lines) and one with the characteristics of the DART mission (red lines) would ensure an effective deviation of the 2011 AG5 asteroid for values of β close to 3. Taking into account the effective value of β in the DART mission ($\beta = 3.6$ [22]), a KI with the characteristics of this mission would have ensured an effective deviation for the 2011 AG5 asteroid as long as the maneuver was performed with sufficient lead time (e.g., with about 20 years in advance, as in the case of Figure 10).

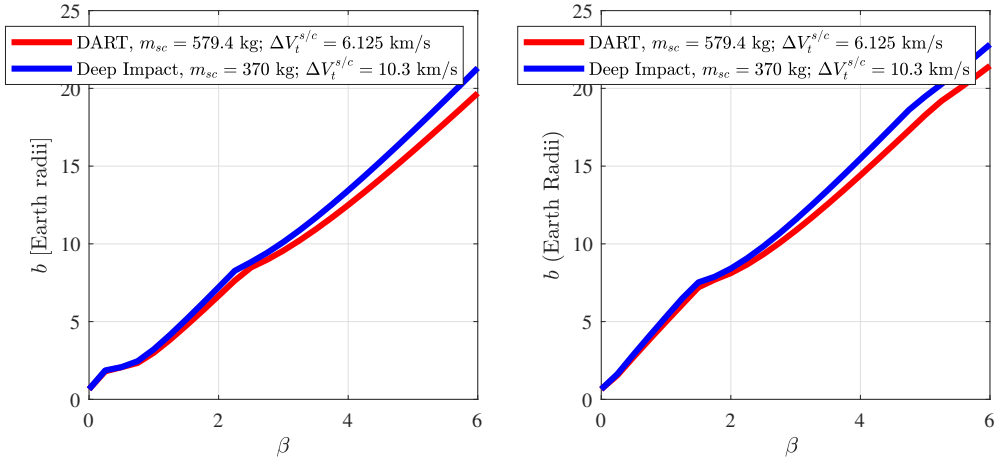

Figure 10. Left panel: effects of a maneuver with positive Δv executed at the perihelion passage on 13 October 2019 using a KI similar to Deep Impact (blue line) and DART (red line) missions. Right panel: same results for negative Δv.

6. Conclusions

The study of NEO 2011 AG5 has been conducted in the context of NEOs with resonant orbits with Earth's heliocentric revolution. Based on orbital element knowledge, numerical integrations that take into account perturbations from main solar system planets have shown that the resonant encounters of the asteroid with Earth do not pose any impact threat until 2040. Therefore, a VI has been obtained by modifying the orbital elements of the asteroid. In particular, two small variations have been applied to the argument of perihelion and mean anomaly, whose effects on MOID and encounter timing lead to a virtual impact in the 2040 resonant passage. In this way, various deflection scenarios have been proposed to avoid impact.

Given the size of 2011 AG5, and the remaining time to virtual impact, the most effective solution is the tried and tested KI. Mission scenarios to deflect 2011 AG5 confirmed commonly held assumptions in the literature. If the two parameters characterizing the spacecraft performance during the maneuver, the KI mass and the relative velocity, have to be considered within certain technological limits, maneuvers at perihelion are more efficient. For example, assuming a performance similar to real missions such as Deep Impact and DART, applying Δv at the 23 October 2019 perihelion would have allowed for deflections of about 10 Earth radii, both accelerating or decelerating the asteroid, with a good chance of avoiding any collision with Earth in 2040. Performing the same maneuver at aphelion or in subsequent perihelion passes, but before the 2023 resonant passage, would result in efficient deflection, provided that the spacecraft mass is increased to $\sim$1000 kg.

Finally, any Δv applied to the asteroid after the 2023 resonant passage would further narrow down the field of efficient maneuvers. This restriction would apply specifically to high mass/relative velocity pairs, requiring an extremely performing launch and spacecraft guidance system. However, deflection of a sufficient number of Earth radii would still be possible.

Funding: This research received no external funding.

Data Availability Statement: No new data were created or analyzed in this study. Data sharing is not applicable to this article.

Acknowledgments: For this work, M. Cinelli has been supported by the G4S_2.0 project, developed under the auspices of the Italian Space Agency (ASI) within the frame of the Bando Premiale CI-COT-2018-085 with the coparticipation of the Italian Institute for Astrophysics (INAF) and the Politecnico di Torino (POLITO). This work was carried out within the National Group for Mathematical Physics (GNFM) of the Italian National Institute of High Mathematics (INdAM).

Conflicts of Interest: The author declares no conflicts of interest.

References

1. Emel'yanenko, V.; Popova, O.; Chugai, N.; Shelyakov, M.; Pakhomov, Y.V.; Shustov, B.; Shuvalov, V.; Biryukov, E.; Rybnov, Y.S.; Marov, M.Y.; et al. Astronomical and physical aspects of the Chelyabinsk event (15 February 2013). *Sol. Syst. Res.* **2013**, *47*, 240–254. [CrossRef]
2. Brown, P.G.; Assink, J.D.; Astiz, L.; Blaauw, R.; Boslough, M.B.; Borovička, J.; Brachet, N.; Brown, D.; Campbell-Brown, M.; Ceranna, L.; et al. A 500-kiloton airburst over Chelyabinsk and an enhanced hazard from small impactors. *Nature* **2013**, *503*, 238–241. [CrossRef] [PubMed]
3. Vasilyev, N.V. The Tunguska meteorite problem today. *Planet. Space Sci.* **1998**, *46*, 129–150. [CrossRef]
4. Alvarez, L.W.; Alvarez, W.; Asaro, F.; Michel, H.V. Extraterrestrial cause for the Cretaceous-Tertiary extinction. *Science* **1980**, *208*, 1095–1108. [CrossRef] [PubMed]
5. Harris, A.W.; D'Abramo, G. The population of near-Earth asteroids. *Icarus* **2015**, *257*, 302–312. [CrossRef]
6. Harris, A.W.; Chodas, P.W. The population of near-earth asteroids revisited and updated. *Icarus* **2021**, *365*, 114452. [CrossRef]
7. Cano, J.L.; Bellei, G.; Martín, J. Integrated end-to-end NEO threat mitigation software suite. In Proceedings of the 64th International Astronautical Congress, Beijing, China, 23–27 September 2013; pp. 23–27.
8. Mainzer, A.; Grav, T.; Bauer, J.; Masiero, J.; McMillan, R.; Cutri, R.; Walker, R.; Wright, E.; Eisenhardt, P.; Tholen, D.; et al. NEOWISE observations of near-Earth objects: Preliminary results. *Astrophys. J.* **2011**, *743*, 156. [CrossRef]
9. Perna, D.; Dotto, E.; Ieva, S.; Barucci, M.; Bernardi, F.; Fornasier, S.; De Luise, F.; Perozzi, E.; Rossi, A.; Epifani, E.M.; et al. Grasping the nature of potentially hazardous asteroids. *Astron. J.* **2015**, *151*, 11. [CrossRef]
10. Schweickart, R.L. Decision program on asteroid threat mitigation. *Acta Astronaut.* **2009**, *65*, 1402–1408. [CrossRef]
11. National Research Council; Division on Engineering and Physical Sciences; Space Studies Board; Aeronautics and Space Engineering Board; Committee to Review Near-Earth-Object Surveys and Hazard Mitigation Strategies. *Defending Planet Earth: Near-Earth-Object Surveys and Hazard Mitigation Strategies*; National Academies Press: Washington, DC, USA, 2010.
12. Kaiser, N.; Aussel, H.; Burke, B.E.; Boesgaard, H.; Chambers, K.; Chun, M.R.; Heasley, J.N.; Hodapp, K.W.; Hunt, B.; Jedicke, R.; et al. Pan-STARRS: A large synoptic survey telescope array. In Proceedings of the Survey and Other Telescope Technologies and Discoveries, Waikoloa, HI, USA, 22–28 August 2002; SPIE: Bellingham, WA, USA, 2002; Volume 4836, pp. 154–164.
13. Ivezić, Ž.; Kahn, S.M.; Tyson, J.A.; Abel, B.; Acosta, E.; Allsman, R.; Alonso, D.; AlSayyad, Y.; Anderson, S.F.; Andrew, J.; et al. LSST: From science drivers to reference design and anticipated data products. *Astrophys. J.* **2019**, *873*, 111. [CrossRef]
14. Rumpf, C.; Lewis, H.G.; Atkinson, P.M. On the influence of impact effect modelling for global asteroid impact risk distribution. *Acta Astronaut.* **2016**, *123*, 165–170. [CrossRef]
15. Dearborn, D.S.; Syal, M.B.; Barbee, B.W.; Gisler, G.; Greenaugh, K.; Howley, K.M.; Leung, R.; Lyzhoft, J.; Miller, P.L.; Nuth, J.A.; et al. Options and uncertainties in planetary defense: Impulse-dependent response and the physical properties of asteroids. *Acta Astronaut.* **2020**, *166*, 290–305. [CrossRef]
16. Cheng, A.F.; Atchison, J.; Kantsiper, B.; Rivkin, A.S.; Stickle, A.; Reed, C.; Galvez, A.; Carnelli, I.; Michel, P.; Ulamec, S. Asteroid impact and deflection assessment mission. *Acta Astronaut.* **2015**, *115*, 262–269. [CrossRef]
17. Thiry, N.; Vasile, M. Statistical multi-criteria evaluation of non-nuclear asteroid deflection methods. *Acta Astronaut.* **2017**, *140*, 293–307. [CrossRef]
18. Schultz, P.H.; Eberhardy, C.A.; Ernst, C.M.; A'Hearn, M.F.; Sunshine, J.M.; Lisse, C.M. The Deep Impact oblique impact cratering experiment. *Icarus* **2007**, *191*, 84–122. [CrossRef]
19. Stickle, A.M.; DeCoster, M.E.; Burger, C.; Caldwell, W.K.; Graninger, D.; Kumamoto, K.M.; Luther, R.; Ormö, J.; Raducan, S.; Rainey, E.; et al. Effects of impact and target parameters on the results of a kinetic impactor: Predictions for the Double Asteroid Redirection Test (DART) mission. *Planet. Sci. J.* **2022**, *3*, 248. [CrossRef]
20. Richardson, J.E.; Melosh, H.J.; Artemeiva, N.A.; Pierazzo, E. Impact cratering theory and modeling for the Deep Impact mission: From mission planning to data analysis. *Space Sci. Rev.* **2005**, *117*, 241–267. [CrossRef]
21. Rivkin, A.S.; Chabot, N.L.; Stickle, A.M.; Thomas, C.A.; Richardson, D.C.; Barnouin, O.; Fahnestock, E.G.; Ernst, C.M.; Cheng, A.F.; Chesley, S.; et al. The double asteroid redirection test (DART): Planetary defense investigations and requirements. *Planet. Sci. J.* **2021**, *2*, 173. [CrossRef]
22. Cheng, A.F.; Agrusa, H.F.; Barbee, B.W.; Meyer, A.J.; Farnham, T.L.; Raducan, S.D.; Richardson, D.C.; Dotto, E.; Zinzi, A.; Della Corte, V.; et al. Momentum transfer from the DART mission kinetic impact on asteroid Dimorphos. *Nature* **2023**, *616*, 457–460. [CrossRef]
23. Daly, R.T.; Ernst, C.M.; Barnouin, O.S.; Chabot, N.L.; Rivkin, A.S.; Cheng, A.F.; Adams, E.Y.; Agrusa, H.F.; Abel, E.D.; Alford, A.L.; et al. Successful kinetic impact into an asteroid for planetary defence. *Nature* **2023**, *616*, 443–447. [CrossRef]
24. Thomas, C.A.; Naidu, S.P.; Scheirich, P.; Moskovitz, N.A.; Pravec, P.; Chesley, S.R.; Rivkin, A.S.; Osip, D.J.; Lister, T.A.; Benner, L.A.; et al. Orbital period change of Dimorphos due to the DART kinetic impact. *Nature* **2023**, *616*, 448–451. [CrossRef]
25. Ketema, Y. Mass-Optimized Gravity Tractor for Asteroid Deflection. *J. Guid. Control. Dyn.* **2022**, *45*, 2318–2331. [CrossRef]
26. Urrutxua, H.; Bombardelli, C.; Hedo, J.M. A preliminary design procedure for an ion-beam shepherd mission. *Aerosp. Sci. Technol.* **2019**, *88*, 421–435. [CrossRef]

27. Bombardelli, C.; Calero, E.J.; Gonzalo, J.L. Deflection of fictitious asteroid 2017 PDC: Ion beam vs. kinetic impactor. *Acta Astronaut.* **2019**, *156*, 301–307. [CrossRef]
28. Bottke, W.F., Jr.; Vokrouhlickỳ, D.; Rubincam, D.P.; Nesvornỳ, D. The Yarkovsky and YORP effects: Implications for asteroid dynamics. *Annu. Rev. Earth Planet. Sci.* **2006**, *34*, 157–191. [CrossRef]
29. Spitale, J.N. Asteroid hazard mitigation using the Yarkovsky effect. *Science* **2002**, *296*, 77. [CrossRef]
30. Syal, M.B.; Owen, J.M.; Miller, P.L. Deflection by kinetic impact: Sensitivity to asteroid properties. *Icarus* **2016**, *269*, 50–61. [CrossRef]
31. DeCoster, M.E.; Rainey, E.S.; Rosch, T.W.; Stickle, A.M. Statistical significance of mission parameters on the deflection efficiency of kinetic impacts: Applications for the next-generation kinetic impactor. *Planet. Sci. J.* **2022**, *3*, 186. [CrossRef]
32. Raducan, S.; Davison, T.; Luther, R.; Collins, G.S. The role of asteroid strength, porosity and internal friction in impact momentum transfer. *Icarus* **2019**, *329*, 282–295. [CrossRef]
33. Yeomans, D.; Bhaskaran, S.; Chesley, S.; Chodas, P.; Grebow, D.; Landau, D.; Petropoulos, S.; Sims, J. *Report on Asteroid 2011 AG5 Hazard Assessment and Contingency Planning*; Jet Propulsion Laboratory, Near Earth Object Program, NASA: Washington, DC, USA, 2012.
34. Lexell, A.J. *Réflexions Sur Le Temps Périodique Des Comètes En Général, Et Principalement Sur Celui De La Comète observée en 1770: Presentées A l'Académie Impériale Des Sciences De St. Petersbourg, Dans Son Assemblée Publique, Du 13. Octobre 1778*; de l'Imprimerie de l'Académie Impériale des Sciences: St. Petersburg, Russia, 1778.
35. Leverrier, U. Annales de l'Observatoire Impérial de Paris. *Mon. Not. R. Astron. Soc.* **1860**, *20*, 303.
36. Milani, A.; Sansaturio, M.E.; Tommei, G.; Arratia, O.; Chesley, S.R. Multiple solutions for asteroid orbits: Computational procedure and applications. *Astron. Astrophys.* **2005**, *431*, 729–746. [CrossRef]
37. Öpik, E.J. Collision probabilities with the planets and the distribution of interplanetary matter. *Proc. R. Ir. Acad. Sect. A Math. Phys. Sci. JSTOR* **1951**, *54*, 165–199.
38. Opik, E.J. Interplanetary encounters: Close-range gravitational interactions. *Amsterdam* **1976**, *2*, 160.
39. Valsecchi, G.B.; Milani, A.; Gronchi, G.F.; Chesley, S.R. Resonant returns to close approaches: Analytical theory. *Astron. Astrophys.* **2003**, *408*, 1179–1196. [CrossRef]
40. Milani, A.; Chesley, S.R.; Valsecchi, G.B. Close approaches of asteroid 1999 AN10: Resonant and non-resonant returns. *Astron. Astrophys.* **1999**, *346*, L65–L68.
41. Chodas, P. The impact threat and public perception. *J. R. Astron. Soc. Can.* **1999**, *93*, 175.
42. Valsecchi, G.; Alessi, E.; Rossi, A. Cartography of the b-plane of a close encounter I: Semimajor axes of post-encounter orbits. *Celest. Mech. Dyn. Astron.* **2018**, *130*, 8. [CrossRef]
43. Carusi, A.; Valsechi, G.; Greenberg, R. Planetary close encounters: Geometry of approach and post-encounter orbital parameters. *Celest. Mech. Dyn. Astron.* **1990**, *49*, 111–131. [CrossRef]
44. Greenberg, R.; Carusi, A.; Valsecchi, G. Outcomes of planetary close encounters: A systematic comparison of methodologies. *Icarus* **1988**, *75*, 1–29. [CrossRef]
45. Valsecchi, G.; Alessi, E.; Rossi, A. An analytical solution for the swing-by problem. *Celest. Mech. Dyn. Astron.* **2015**, *123*, 151–166. [CrossRef]
46. Gronchi, G.; Milani, A. Proper elements for Earth-crossing asteroids. *Icarus* **2001**, *152*, 58–69. [CrossRef]
47. Folkner, W.M.; Williams, J.G.; Boggs, D.H.; Park, R.S.; Kuchynka, P. The planetary and lunar ephemerides DE430 and DE431. *Interplanet. Netw. Prog. Rep.* **2014**, *196*, 42–196.
48. Bellei, G.; Cano, J. *Kinetic Impact Mitigation Options for Asteroid 2011 AG5*; Deimos Space, Elecnor Deimos: Tres Cantos, Spain, 2012.
49. Ahrens, T.J.; Harris, A.W. *Hazards Due to Comets and Asteroids*; University of Arizona Press: Tucson, AZ, USA, 1994.
50. Holsapple, K.A. About deflecting asteroids and comets. In *Mitigation of Hazardous Comets and Asteroids*; Cambridge University Press: Cambridge, UK, 2004; pp. 113–140.
51. Scheeres, D.J.; McMahon, J.W.; Jones, B.A.; Doostan, A. Variation of delivered impulse as a function of asteroid shape. In Proceedings of the 2015 IEEE Aerospace Conference, Big Sky, MT, USA, 7–14 March 2015; IEEE: Piscataway, NJ, USA, 2015; pp. 1–7.
52. Grebow, D.; Landau, D.; Bhaskaran, S.; Chodas, P.; Chesley, S.; Yeomans, D.; Petropoulos, A.; Sims, J. *Deflection Missions for asteroid 2011 AG5*; California Institute of Technology: Pasadena, CA, USA, 2012.
53. A'Hearn, M.F.; Belton, M.; Delamere, W.; Kissel, J.; Klaasen, K.; McFadden, L.; Meech, K.; Melosh, H.; Schultz, P.; Sunshine, J.; et al. Deep impact: Excavating comet Tempel 1. *Science* **2005**, *310*, 258–264. [CrossRef] [PubMed]
54. Cheng, A.F.; Rivkin, A.S.; Michel, P.; Atchison, J.; Barnouin, O.; Benner, L.; Chabot, N.L.; Ernst, C.; Fahnestock, E.G.; Kueppers, M.; et al. AIDA DART asteroid deflection test: Planetary defense and science objectives. *Planet. Space Sci.* **2018**, *157*, 104–115. [CrossRef]
55. Housen, K.R.; Holsapple, K.A. Ejecta from impact craters. *Icarus* **2011**, *211*, 856–875. [CrossRef]
56. Hoerth, T.; SchÄFer, F.; Thoma, K.; Kenkmann, T.; Poelchau, M.H.; Lexow, B.; Deutsch, A. Hypervelocity impacts on dry and wet sandstone: Observations of ejecta dynamics and crater growth. *Meteorit. Planet. Sci.* **2013**, *48*, 23–32. [CrossRef]
57. Biver, N.; Bockelée-Morvan, D.; Boissier, J.; Crovisier, J.; Colom, P.; Lecacheux, A.; Moreno, R.; Paubert, G.; Lis, D.C.; Sumner, M.; et al. Radio observations of Comet 9P/Tempel 1 before and after Deep Impact. *Icarus* **2007**, *191*, 494–512. [CrossRef]